

Accurate modeling of FeSe with screened Fock exchange and Hund metal correlations

Tommaso Gorni ¹, Pablo Villar Arribi ¹, Michele Casula ² and Luca de' Medici¹

¹*LPEM, ESPCI Paris, PSL Research University, CNRS, Sorbonne Université, 75005 Paris France*

²*Institut de Minéralogie, de Physique des Matériaux et de Cosmochimie (IMPMC), Sorbonne Université, CNRS UMR 7590, IRD UMR 206, MNHN, 4 Place Jussieu, 75252 Paris, France*



(Received 15 January 2021; revised 17 June 2021; accepted 24 June 2021; published 14 July 2021)

We reproduce the electronic properties of FeSe in the high-temperature phase within an *ab initio* framework that includes screened Fock exchange and local dynamical correlations. We robustly capture the experimental band structure, as long as the system is in the Hund metal phase. In particular, we account for the shrinking of the Fermi pockets and the sinking below the Fermi level of the hole pocket with *xy* orbital character. This entails the elusive correct estimate of the Sommerfeld coefficient, and supports the interpretation of noncompensated Fermi pockets seen in ARPES in terms of surface electron doping. More stringently, our modeling matches well the experimental interband optical spectrum, and captures qualitatively the temperature dependence of the thermoelectric power, extremely sensitive to the details of the bands around the Fermi level.

DOI: [10.1103/PhysRevB.104.014507](https://doi.org/10.1103/PhysRevB.104.014507)

More than ten years after their discovery [1], consensus on the physics of iron-based superconductors (IBSC) is yet to be reached. Albeit there are substantial indications pointing towards a spin-fluctuation pairing mechanism for superconductivity induced by the proximity to magnetic instabilities [2–4], many important features are still not understood, such as the nature of the nematic symmetry breaking, occurring in the normal state of many compounds, or the prediction of material trends. In order to reach these goals, an accurate material-specific description of their electronic structure is essential.

Density-functional theory (DFT) in its standard implementations [the local-density approximation (LDA) or the generalized gradient approximation (GGA)] qualitatively reproduces the structure of the Fermi surface, i.e., that of a semimetal (compensated in the parent compounds) with hole pockets in the center of the Brillouin zone and electron pockets at the corners [5]. Nonetheless, quantitative mismatches are found when the calculated Fermi surfaces are compared with angle-resolved photoemission spectroscopy (ARPES) or quantum oscillation measurements throughout all the IBSC families [6–10]. Moreover, the DFT electronic bands are at least a factor 2 to 3 more dispersive than what found experimentally, with a simple rescaling of the DFT bandwidth not being enough to reach agreement with the experimental findings [11].

This bandwidth mismatch can be ascribed to the lack of local dynamical correlations induced by local interactions and in particular by the Hund coupling—the intra-atomic exchange—within the DFT framework. These interactions have been shown to induce a strongly correlated metallic phase in IBSC, dominated by fluctuating local high-spin configurations and therefore dubbed as *Hund metal* [12–14], in which electronic correlations strongly renormalize the bands in an orbitally differentiated, thus highly nontrivial, way [12,15–19]. For this reason dynamical mean-field theory

(DMFT), and even the simpler Gutzwiller or slave-particle methods, drastically improve the overall band structure, and more generally electronic and magnetic properties, with respect to a plain DFT description [12,20,21].

The combinations of these methods with LDA- or GGA-derived models, however, are not able to explain or reproduce some fundamental features, e.g., the size of electron and hole pockets of the Fermi surface [12]. This issue is particularly striking in tetragonal FeSe, whose experimentally measured hole pocket is from five to six times smaller than the one predicted by both standard DFT or DFT+DMFT calculations [10,16,22,23]. Two main mechanisms have been proposed to cure this inaccuracy, one mediated by dynamical fluctuations [24,25], the other as a static effect of the intersite Coulomb repulsion treated at the Hartree-Fock level [26,27]. Up to now, the lack of a detailed comparison with experiments of an *ab initio* description of FeSe's normal phase has not allowed us to clearly discriminate between the two scenarios.

In this work we tackle the *ab initio* modeling of FeSe and we show that an accurate description of the Fermi surfaces can be obtained by including screened Fock exchange effects in the reference Hamiltonian via *hybrid functional* DFT [28,29]. Moreover, by including as well local dynamical correlations due to the Hund metallicity, we obtain a quasiparticle band structure matching quite accurately (both in dispersion and orbital character) ARPES and transport experimental measurements. Our result thus supports the static mechanism for the shrinking of the Fermi pockets in this material, and more in general the nontrivial disentanglement of the electronic self-energy into a static nonlocal and a dynamical local component, i.e.

$$\Sigma(\mathbf{k}, \omega) = \Sigma_{\text{nonloc}}(\mathbf{k}) + \Sigma_{\text{dyn}}(\omega), \quad (1)$$

to a good level of approximation, in line with earlier *GW* calculations on IBSC [30,31] and oxides [32], SEX+DMFT

calculations on cobalt pnictides [33], and a more recent analysis of ARPES experimental data [34].

I. METHODS

We calculate a reference one-body DFT Hamiltonian using both the Perdew-Burke-Ernzerhof (PBE) GGA functional [35] and the HSE hybrid functional [36,37], which admixes a fraction of short-range Hartree-Fock exchange energy into the PBE exchange energy. All the DFT calculations have been carried out using the experimental lattice parameters $a = 3.7707 \text{ \AA}$, $c = 5.521 \text{ \AA}$, and $z_{\text{Se}} = 0.2667$ for the tetragonal phase of FeSe [38,39], using the QUANTUM ESPRESSO package [40–42].

As in all IBSC, the bands crossing the Fermi level in FeSe are mainly of Fe-3*d* character, and in order to include many-body effects through the explicit treatment of local correlations, a parametrization of the one-body Hamiltonian on a localized basis is necessary. We thus project the DFT Kohn-Sham Hamiltonian over a set of five maximally localized Wannier functions per Fe site, using the WANNIER90 code [43]. This downfolding process yields the hopping and on-site energies of the one-body part

$$\hat{\mathcal{H}}_0 = \sum_{i \neq j, m, m', \sigma} t_{ij}^{mm'} \hat{d}_{im\sigma}^\dagger \hat{d}_{jm'\sigma} + \sum_{i, m, \sigma} \epsilon_{im\sigma} \hat{n}_{im\sigma}, \quad (2)$$

where $\hat{d}_{im\sigma}^\dagger$ creates an electron in the Wannier spin-orbital $m\sigma$ centered at the lattice site i , and $\hat{n}_{im\sigma} = \hat{d}_{im\sigma}^\dagger \hat{d}_{im\sigma}$ is the corresponding number operator.

A Hubbard-Kanamori Hamiltonian is used to include the local interactions to be treated in a dynamical many-body fashion:

$$\begin{aligned} \hat{\mathcal{H}} = \hat{\mathcal{H}}_0 + U \sum_{i, m} \hat{n}_{im\uparrow} \hat{n}_{im\downarrow} + (U - 2J) \sum_{i, m \neq m'} \hat{n}_{im\uparrow} \hat{n}_{im'\downarrow} \\ + (U - 3J) \sum_{i, m < m', \sigma} \hat{n}_{im\sigma} \hat{n}_{im'\sigma}, \end{aligned} \quad (3)$$

where U is the intraorbital Coulomb repulsion and J is the Hund coupling [44]. In this framework the double counting energy for these interactions is absorbed in the chemical potential.

Here we solve the many-body Hamiltonian (3) within the slave-spin mean-field theory (SSMF) [45,46], which treats many-body effects in a simpler way than DMFT, yet providing a $\Sigma_{\text{dyn}}(\omega)$ which has proven to be a robust approximation for IBSC by, e.g., successfully capturing their orbital-differentiation signatures [19], or predicting the evolution of the Sommerfeld coefficient upon doping in the 122 family [47]. SSFM describes the Fermi-liquid low-temperature paramagnetic metallic phase of (3) as a quasiparticle Hamiltonian

$$\begin{aligned} \hat{\mathcal{H}}_{\text{QP}} = \sum_{i \neq j, m, m', \sigma} \sqrt{Z_m Z_{m'}} t_{ij}^{mm'} \hat{f}_{im\sigma}^\dagger \hat{f}_{jm'\sigma} \\ + \sum_{i, m, \sigma} (\epsilon_m - \tilde{\lambda}_m) \hat{n}_{im\sigma}^f, \end{aligned} \quad (4)$$

where the (orbital-dependent) quasiparticle renormalizations Z_m and on-site-energy shifts $\tilde{\lambda}_m$ are determined solving the

self-consistent slave-spin equations for given values of the local interactions U and J [42,46].

When building the reference Hamiltonian \mathcal{H}_0 starting from the PBE Kohn-Sham states (we label the final result SSMF@PBE), we set $U^{\text{PBE}} = 4.2 \text{ eV}$ and $J^{\text{PBE}} = 0.2 U^{\text{PBE}}$, based on constrained random-phase approximation calculations (cRPA) [48], and benchmarking on higher-level theories [42]. In the HSE case (labeled SSMF@HSE), we keep the same J/U ratio as for PBE, and we fix $U^{\text{HSE}} = 5.0 \text{ eV}$, the value at which the t_{2g} mass renormalization is closest to the SSMF@PBE one. This choice is further validated by performing several scans in the (U, J) space, showing that the main improvements with respect to the SSMF@PBE case are robust with respect to changes in the local interactions, as long as the system is within the Hund metal phase. This is indeed a region of strong and orbitally differentiated mass renormalization, which is systematically found in these models at interaction strengths beyond a crossover value [14,49–53] (see the blue-shaded region in the bottom panels in Fig. 1).

II. QUASIPARTICLE DISPERSION AND FERMION SURFACE

The itinerant-fermion description of FeSe yielded by the PBE (or LDA) functional is known to predict an overall correct shape of the Fermi surface, but also to overestimate the hole-pocket size of about a factor 5 and underestimate the effective masses up to 8 times [10,55]. For this reason, the PBE bands shown in the upper panel of Fig. 1 are renormalized by a constant factor $Z = 1/6$, so to ease the comparison of their dispersion with the subsequent cases. It must be noted, however, that this simple rigid renormalization does not account for the quasiparticle mass differentiation reported in experiments, with values of $m^*/m_b = 1/Z$ ranging from 2–3 for the xz/yz bands up to 8 for the xy bands, with m_b being the PBE masses [10]. The mass differentiation is naturally brought in by the dynamical local correlations in the Hund metal region along with the strong overall renormalization, as shown by our SSMF@PBE calculations presented in the upper-middle panel in Fig. 1. However, regardless of the methodology used, local self-energies alone do not improve the PBE Fermi surface, yielding Fermi pockets of roughly the same size as PBE and an over-representation of the xy character [16,22,23], in stark contrast with experimental evidence [10,54,56].

The main outcome of this work is reported in the lower-middle panel of Fig. 1, displaying the band structure and Fermi surface obtained with SSMF when using the HSE reference Hamiltonian. When the HSE static screened Fock exchange is included in the quasiparticle equations, the xy band sinks below the Fermi level at the zone center, leaving a smaller hole pocket of xz/yz character and explaining the origin of the flat band seen in ARPES about 50 meV below ϵ_F [10,57]. At the zone corner, a relevant xy weight remains in the outermost part of elliptical pockets, in agreement with recent polarized-ARPES data [54], and the xy and xz/yz bands form together a double-hourglass shape with band bottoms at 60 and 30 meV below ϵ_F , consistently with their experimental position of about 50–60 meV and 20–40 meV below ϵ_F , respectively [10,25,56,58,59].

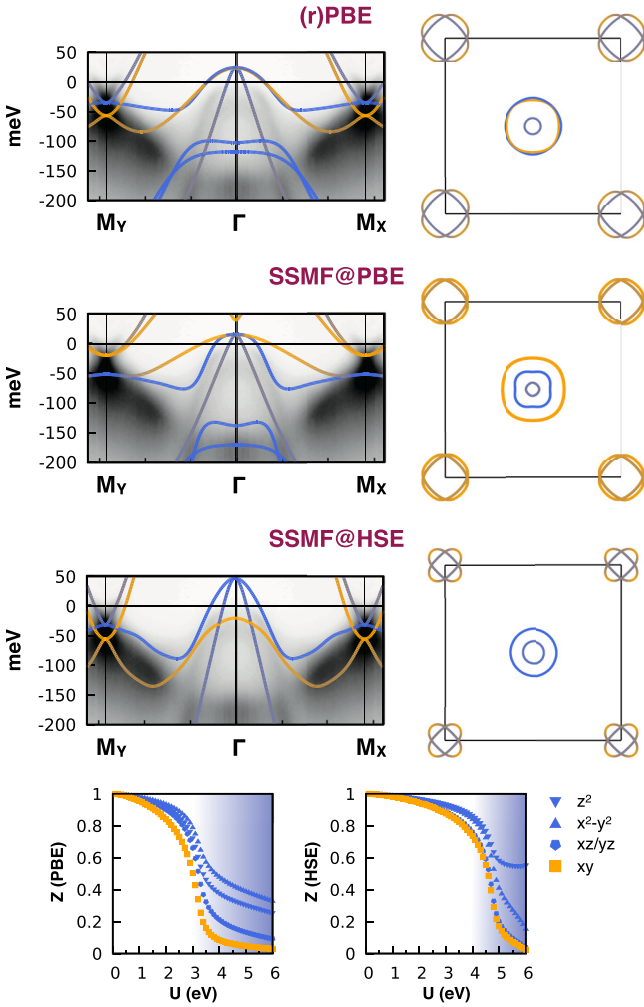


FIG. 1. Calculated band dispersion along the M_y - Γ - M_x path (solid lines) on top of the corresponding ARPES dispersions from Ref. [54] (grayscale), and $k_z = 0$ Fermi surface of FeSe, shown in the 2-Fe Brillouin zone. The xy orbital weight is represented in a color scale going from blue (zero weight) to orange (maximum weight). Upper panel: PBE case renormalized by a constant factor $1/Z = 6$. Upper-middle panel: SSMF@PBE solution with local interaction parameters $U = 4.2$ eV and $J/U = 0.20$. Lower-middle panel: SSMF@HSE solution with local interaction parameters $U = 5.0$ eV and $J/U = 0.20$. Only the latter reproduces correctly the shrinking of the Fermi pockets, the sinking of the xy band at Γ , and the band dispersions. In the two bottom panels, the SSMF mass renormalizations for fixed $J/U = 0.20$ are reported for both reference Hamiltonians considered. The Hund metal region is shaded in blue.

A crucial consequence of this band rearrangement is the net reduction of the size of the Fermi pockets, pointing towards static nonlocal Coulomb effects as the most likely pocket-shrinking mechanism in FeSe. Furthermore, the competing dynamical nonlocal scenario has been recently shown to be quite ineffective in FeSe, even when accounting for realistic nonlocal dynamical fluctuations [60]. We remark that the observed Fermi surface shrinking is a multiband effect, with the xz/yz pockets being more sensitive to local dynamical correlations and the xy pockets more affected by nonlocal static

effects, as long as the local correlations are strong enough to place FeSe in the Hund metal phase [42].

Finally, a relevant point that has never been explicitly addressed in the literature to our knowledge is the lack of compensation (between the volumes of the hole and electron pockets, due to the Luttinger theorem for Fermi liquids) inferred from ARPES measurements (see Table 1 in the Supplemental Material [42]). The experimentally reported volumes of the xz/yz electron and hole pockets tend to compensate one another, therefore the volume of the xy electron pocket is expected to be compensated by a corresponding hole pocket, which however has always escaped detection. The general difficulty in resolving the xy bands in ARPES [25], together with the prediction of a high xy scattering rate [16], may lead to the conjecture that a faint, undetected xy hole pocket is indeed present at the zone center. However, the stark improvement in our calculated band structure produced by the xy hole pocket sinking below the Fermi level, together with the clear experimental detection of an xy band in the same energy range in the low temperature phase [10], lead us to discard the occurrence of an xy hole pocket in FeSe, and to propose surface electron doping as the most likely explanation to the lack of compensation in ARPES experiments. A precise quantification of this doping would necessitate us to account for finer energy scale effects such as spin-orbit coupling and is beyond the scope of this study, we thus limit ourselves to estimate that a rigid shift of the chemical potential in the SSMF@HSE band structure reproduces the experimental pocket sizes for an electron doping of about $0.1e^-$ per Fe.

III. SPECIFIC HEAT

We now turn to the Sommerfeld coefficient γ_n , i.e., the linear coefficient in the electronic specific heat as a function of temperature. The Sommerfeld coefficient is proportional to the bulk density of states (DoS) at the Fermi level, which is ultimately a sensitive probe of the renormalized band structure and thus of electronic correlations [61]. Even though the FeSe tetragonal phase is not stable below 90 K, hampering a precise extrapolation of the specific heat to zero temperature, a rough estimate of its Sommerfeld coefficient can be inferred based on the low-temperature phase measurements, leading to a value of about $\gamma_n \approx 12$ mJ mol $^{-1}$ K $^{-2}$ [62,63]. Comparing with the ones predicted theoretically within the different schemes, SSMF@HSE yields $\gamma_n = 9.0$ mJ mol $^{-1}$ K $^{-2}$, in much closer agreement with the experimental estimate than the SSMF@PBE value of $\gamma_n = 36.6$ mJ mol $^{-1}$ K $^{-2}$, or than the (unrenormalized) PBE value of $\gamma_n = 4.0$ mJ mol $^{-1}$ K $^{-2}$. The difference between the two correlated cases can again be traced back to the xy band, whose positioning below the Fermi level is further supported by this estimation.

IV. TRANSPORT PROPERTIES

In order to assess the quality of our band structure over a broader energy range, we compute the optical conductivity of tetragonal FeSe. Neglecting vertex corrections, its real part

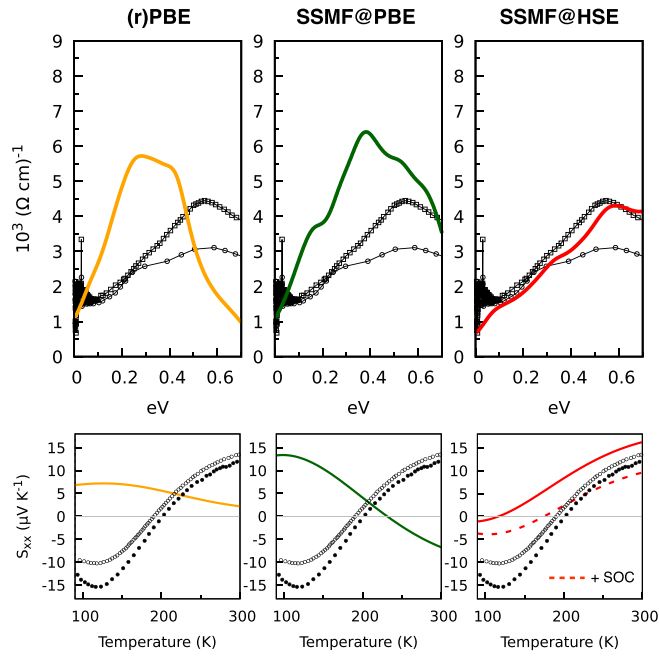


FIG. 2. In-plane interband contribution to the optical conductivity (upper panels) and thermopower (lower panels) of FeSe, computed in the renormalized-PBE, SSMF@PBE, and SSMF@HSE cases. Optical conductivity calculations (solid lines, upper panels) are compared with the experimental data for 205-nm-FeSe@CaF₂ at $T = 100$ K [64] (open circles), and for a FeSe monocrystal at $T = 120$ K [65] (open squares), both subtracted of their coherent Drude peak. A Lorentzian broadening $\eta = 0.06$ eV has been used in the computation of the theoretical spectra. Thermopower calculations (solid lines, lower panels) are compared with experimental data of FeSe polycrystals (open circles from [66], full circles from [67]), for the temperature range above the nematic transition, occurring around $T = 90$ K at ambient pressure [68].

reads as

$$\text{Re}[\sigma_{\alpha\beta}(\omega)] = \frac{2\pi e^2 \hbar}{V} \sum_k^{\text{BZ}} \int_{-\infty}^{+\infty} d\omega' \frac{f(\omega') - f(\omega + \omega')}{\omega} \times \text{Tr}[v_{k\alpha} A_k(\omega') v_{k\beta} A_k(\omega + \omega')], \quad (5)$$

where $f(\omega)$ is the Fermi function, $A_k(\omega)$ is the spectral function matrix, and $v_{k\alpha}^{mm'}$ are the velocity matrix elements computed within the Peierls approximation [69,70]. Within SSMF quasiparticles have infinite lifetime, which implies an unbroadened Drude peak in optics, an artificial feature in this context. We thus examine only the interband contributions to the optical conductivity [71], so to avoid empirical fittings of the Drude width. In the upper panels of Fig. 2 we report the interband contribution to the in-plane optical conductivity (i.e., in the Fe-Fe plane, along the Fe-Se direction) in the renormalized-PBE, SSMF@PBE, and SSMF@HSE case. Optical conductivity data in IBSC are usually interpreted by means of two different Drude peaks, describing, respectively, the coherent and incoherent electron dynamics. We choose to subtract only the coherent Drude peak to the experimental data, since the experimentally fitted incoherent one, with a broadening of $\hbar/\tau \approx 0.2$ eV [64], might include portions of

interband transitions. From the upper panels of Fig. 2 one can see that SSMF@HSE better reproduces the experimental trends, predicting a main absorption around 0.6 eV and a secondary one around 0.3 eV. The higher-energy transition is detected both in the FeSe monocrystal [65], around $\hbar\omega_0 \approx 0.55$ eV at $T = 120$ K, and in 205-nm-FeSe@CaF₂ [64], around $\hbar\omega_0 \approx 0.62$ eV at $T = 100$ K, whereas a less intense interband transition is reported in 205-nm-FeSe@CaF₂ around $\hbar\omega_0 \approx 0.25$ eV at $T = 100$ K. On the contrary, both the renormalized-PBE and SSMF@PBE optics yield an excessively intense absorption peak between 0.3–0.4 eV, highlighting the crucial role played by screened Fock exchange in reproducing not only the band structure in detail but also the bands orbital character, which shapes—through the velocity matrix elements—the interband optical conductivity. We finally notice that in the SSMF@HSE case a fainter interband absorption around 0.1 eV is present and not reported by either experiment. Its intensity and position suggest that it might have been incorporated into the empirically-fitted incoherent Drude peak, with a consequent overestimation of its intensity.

The Seebeck effect, i.e., the induction of a charge current due to a thermal gradient, is a phenomenon sensitive to the details of the electronic structure within the thermal energy windows, making thermopower measurements a standard probe for Fermi surface reconstructions and related low-energy properties [72]. For the same reason, it provides a very challenging playground for theoretical predictions, where even the qualitative agreement has not to be taken for granted [73]. In a system showing no transverse current response, the thermopower is a diagonal tensor reading as

$$S_{\alpha\alpha}(T) = -\frac{1}{eT} \frac{\int d\epsilon (\epsilon - \mu) \left(-\frac{\partial f}{\partial \epsilon}\right) \Xi_{\alpha\alpha}(\epsilon)}{\int d\epsilon \left(-\frac{\partial f}{\partial \epsilon}\right) \Xi_{\alpha\alpha}(\epsilon)}, \quad (6)$$

where e is the absolute value of the electron charge, and both the chemical potential μ and the derivative of the Fermi function $f(\epsilon)$ are meant at their temperature- T value. The integrals in Eq. (6) involve the transport distribution function $\Xi_{\alpha\beta}(\epsilon) = \frac{2\pi\hbar}{V} \sum_k \text{Tr}[v_{k\alpha} A_k(\epsilon) v_{k\beta} A_k(\epsilon)]$ that we evaluate within SSMF. This is a quite rough approximation, since it implies a constant relaxation time that simplifies between numerator and denominator in Eq. (6). Furthermore, we neglect phonon-drag effects. The in-plane thermopower as a function of temperature is shown in the lower panels of Fig. 2, compared with experimental data on polycrystalline samples. Local correlations alone are unable to predict the correct trend and sign over the whole temperature range, whereas the inclusion of screened Fock exchange (SSMF@HSE) restores the correct behavior below room temperature, where the agreement with experiments is closer, and predicts a change of sign within the tetragonal phase when lowering the temperature. The agreement with the experimental data deteriorates as T decreases, which can be partially explained by the lack of spin-orbit coupling (SOC) in our calculations. Indeed, band splittings up to 20 meV have been related to SOC in FeSe [10,25,57,74,75], enough to affect the low-temperature behavior of the Seebeck coefficient (see dashed line in the last panel of Fig. 2 and Supplementary Material [42]).

V. CONCLUSIONS

In summary, we have shown that the inclusion of screened Fock exchange in DFT, through the HSE hybrid functional, and of local Hund metal correlations within the slave-spin mean field theory, yields a remarkably accurate description of the band structure of FeSe. Compared to the standard PBE approximation, using the HSE reference Hamiltonian induces a shrinking of the Fermi pockets, bringing their size closer to the experimental values, and generally improves the description of the renormalized quasiparticle bands and of transport properties. We remark that our SSMF@HSE approach is arguably the numerically cheapest way to incorporate all the main physical effects necessary for an accurate description of FeSe, with respect to the more complete but computationally heavier $GW+DMFT$ [30] or $SEX+DMFT$ [33].

Our results suggest that the lack of compensation in ARPES data may be due to surface electron doping, and point towards static short-range Coulomb effects to be the most

likely mechanism for pocket shrinking in FeSe. Finally, our findings support the conjecture that nonlocal and dynamical effects can be disentangled in the self-energy of IBSC to a good level of approximation [30,31,34].

ACKNOWLEDGMENTS

The authors acknowledge fruitful discussions with V. Brouet, L. Fanfarillo, A. Georges, F. Hardy, L. Paulatto, and S. Pons. T.G., P.V.A., and L.d.M. are supported by the European Commission through the ERC-CoG2016, Strong-CoPhy4Energy, GA No724177. This work was performed using HPC resources from GENCI-IDRIS/TGCC (Grants No. A0060910777 and No. 0906493). This work was granted access to the HPC resources of MesoPSL financed by the Region Île-de-France and the project Equip@Meso (Reference No. ANR-10-EQPX-29-01) of the programme Investissements d'Avenir supervised by the Agence Nationale pour la Recherche.

-
- [1] Y. Kamihara, T. Watanabe, M. Hirano, and H. Hosono, *J. Am. Chem. Soc.* **130**, 3296 (2008).
- [2] I. I. Mazin, D. J. Singh, M. D. Johannes, and M. H. Du, *Phys. Rev. Lett.* **101**, 057003 (2008).
- [3] P. J. Hirschfeld, *C. R. Phys.* **17**, 197 (2016).
- [4] A. Chubukov, in *Iron-Based Superconductivity*, edited by D. P. Johnson, G. Xu, and W.-G. Yin (Springer International, Cham, 2015), pp. 255–329.
- [5] Y. Zhang, Z. R. Ye, and D. L. Feng, in *Iron-Based Superconductivity*, edited by P. D. Johnson, G. Xu, and W.-G. Yin (Springer International, Cham, 2015), pp. 115–149.
- [6] A. Coldea, J. Fletcher, A. Carrington, J. Analytis, A. Bangura, J.-H. Chu, A. Erickson, I. Fisher, N. Hussey, and R. McDonald, *Phys. Rev. Lett.* **101**, 216402 (2008).
- [7] V. Brouet, M. Marsi, B. Mansart, A. Nicolaou, A. Taleb-Ibrahimi, P. Le Fevre, F. Bertran, F. Rullier-Albenque, A. Forget, and D. Colson, *Phys. Rev. B* **80**, 165115 (2009).
- [8] G. Lee, H. S. Ji, Y. Kim, C. Kim, K. Haule, G. Kotliar, B. Lee, S. Khim, K. H. Kim, K. S. Kim *et al.*, *Phys. Rev. Lett.* **109**, 177001 (2012).
- [9] T. Terashima, N. Kurita, M. Kimata, M. Tomita, S. Tsuchiya, H. Satsukawa, A. Harada, K. Hazama, M. Imai, A. Sato *et al.*, *J. Phys. Conf. Ser.* **449**, 012022 (2013).
- [10] M. D. Watson, T. K. Kim, A. A. Haghighirad, N. R. Davies, A. McCollam, A. Narayanan, S. F. Blake, Y. L. Chen, S. Ghannadzadeh, A. J. Schofield, M. Hoesch, C. Meingast, T. Wolf, and A. I. Coldea, *Phys. Rev. B* **91**, 155106 (2015).
- [11] H. Ding, K. Nakayama, P. Richard, S. Souma, T. Sato, T. Takahashi, M. Neupane, Y.-M. Xu, Z.-H. Pan, A. V. Fedorov, Z. Wang, X. Dai, Z. Fang, G. F. Chen, J. L. Luo, and N. L. Wang, *J. Phys.: Condens. Matter* **23**, 135701 (2011).
- [12] Z. Yin, K. Haule, and G. Kotliar, *Nat. Mater.* **10**, 932 (2011).
- [13] A. Georges, L. de' Medici, and J. Mravlje, *Annu. Rev. Condens. Matter Phys.* **4**, 137 (2013).
- [14] L. de' Medici, *Hund's Metals Explained*, edited by E. Pavarini, E. Koch, R. Scalettar, and R. Martin, The Physics of Correlated Insulators, Metals, and Superconductors Modeling and Simulation (Forschungszentrum, Juelich, 2017), Vol. 7.
- [15] L. de' Medici, S. R. Hassan, M. Capone, and X. Dai, *Phys. Rev. Lett.* **102**, 126401 (2009).
- [16] M. Aichhorn, S. Biermann, T. Miyake, A. Georges, and M. Imada, *Phys. Rev. B* **82**, 064504 (2010).
- [17] L. de' Medici, *Phys. Rev. B* **83**, 205112 (2011).
- [18] R. Yu and Q. Si, *Phys. Rev. B* **86**, 085104 (2012).
- [19] L. de' Medici, G. Giovannetti, and M. Capone, *Phys. Rev. Lett.* **112**, 177001 (2014).
- [20] P. Hansmann, R. Arita, A. Toschi, S. Sakai, G. Sangiovanni, and K. Held, *Phys. Rev. Lett.* **104**, 197002 (2010).
- [21] P. Werner, M. Casula, T. Miyake, F. Aryasetiawan, A. J. Millis, and S. Biermann, *Nat. Phys.* **8**, 331 (2012).
- [22] I. Leonov, S. Skornyakov, V. Anisimov, and D. Vollhardt, *Phys. Rev. Lett.* **115**, 106402 (2015).
- [23] M. D. Watson, S. Backes, A. A. Haghighirad, M. Hoesch, T. K. Kim, A. I. Coldea, and R. Valentí, *Phys. Rev. B* **95**, 081106 (2017).
- [24] L. Ortenzi, E. Cappelluti, L. Benfatto, and L. Pietronero, *Phys. Rev. Lett.* **103**, 046404 (2009).
- [25] L. Fanfarillo, J. Mansart, P. Toulemonde, H. Cercellier, P. Le Fèvre, F. Bertran, B. Valenzuela, L. Benfatto, and V. Brouet, *Phys. Rev. B* **94**, 155138 (2016).
- [26] K. Jiang, J. Hu, H. Ding, and Z. Wang, *Phys. Rev. B* **93**, 115138 (2016).
- [27] D. D. Scherer, A. Jacko, C. Friedrich, E. Şaşıoğlu, S. Blügel, R. Valentí, and B. M. Andersen, *Phys. Rev. B* **95**, 094504 (2017).
- [28] M. Marsman, J. Paier, A. Stroppa, and G. Kresse, *J. Phys.: Condens. Matter* **20**, 064201 (2008).
- [29] C. Franchini, *J. Phys.: Condens. Matter* **26**, 253202 (2014).
- [30] J. M. Tomczak, M. Van Schilfgaarde, and G. Kotliar, *Phys. Rev. Lett.* **109**, 237010 (2012).
- [31] J. M. Tomczak, *J. Phys. Conf. Ser.* **592**, 012055 (2015).
- [32] J. M. Tomczak, M. Casula, T. Miyake, and S. Biermann, *Phys. Rev. B* **90**, 165138 (2014).
- [33] A. van Roekeghem, T. Ayrál, J. M. Tomczak, M. Casula, N. Xu, H. Ding, M. Ferrero, O. Parcollet, H. Jiang, and S. Biermann, *Phys. Rev. Lett.* **113**, 266403 (2014).

- [34] M. Kim, H. Miao, S. Choi, M. Zingl, A. Georges, and G. Kotliar, *Phys. Rev. B* **103**, 155107 (2021).
- [35] J. P. Perdew, K. Burke, and M. Ernzerhof, *Phys. Rev. Lett.* **77**, 3865 (1996).
- [36] J. Heyd, G. E. Scuseria, and M. Ernzerhof, *J. Chem. Phys.* **118**, 8207 (2003).
- [37] J. Heyd, G. E. Scuseria, and M. Ernzerhof, *J. Chem. Phys.* **124**, 219906 (2006).
- [38] S. Margadonna, Y. Takabayashi, M. T. McDonald, K. Kasperkiewicz, Y. Mizuguchi, Y. Takano, A. N. Fitch, E. Suard, and K. Prassides, *Chem. Commun.* **2008**, 5607 (2008).
- [39] M. Lehman *et al.*, *J. Phys. Conf. Ser.* **251**, 012009 (2010).
- [40] P. Giannozzi, S. Baroni, N. Bonini, M. Calandra, R. Car, C. Cavazzoni, D. Ceresoli, G. Chiarotti, M. Cococcioni, I. Dabo, A. Dal Corso, S. De Gironcoli, S. Fabris, G. Fratesi, R. Gebauer, U. Gerstmann, C. Gougoussis, A. Kokalj, M. Lazzeri, L. Martin-Samos *et al.*, *J. Phys.: Condens. Matter* **21**, 395502 (2009).
- [41] P. Giannozzi, O. Andreussi, T. Brumme, O. Bunau, M. Buongiorno Nardelli, M. Calandra, R. Car, C. Cavazzoni, D. Ceresoli, M. Cococcioni, N. Colonna, I. Carnimeo, A. Dal Corso, S. de Gironcoli, P. Delugas, R. A. DiStasio Jr., A. Ferretti, A. Floris, G. Fratesi, G. Fugallo *et al.*, *J. Phys.: Condens. Matter* **29**, 465901 (2017).
- [42] See Supplemental Material at <http://link.aps.org/supplemental/10.1103/PhysRevB.104.014507> for additional information on DFT calculations [76–79], details on the SSMF method [18,50,80–82], and ARPES data [83,84].
- [43] G. Pizzi, V. Vitale, R. Arita, S. Blügel, F. Freimuth, G. Géranton, M. Gibertini, D. Gresch, C. Johnson, T. Koretsune *et al.*, *J. Phys.: Condens. Matter* **32**, 165902 (2020).
- [44] Here the local off-diagonal terms of the Kanamori Hamiltonian (spin flip and pair hopping) are customarily dropped.
- [45] L. de’ Medici, A. Georges, and S. Biermann, *Phys. Rev. B* **72**, 205124 (2005).
- [46] L. de’ Medici and M. Capone, in *The Iron Pnictide Superconductors: An Introduction and Overview*, edited by F. Mancini and R. Citro (Springer International, Cham, 2017), pp. 115–185.
- [47] F. Hardy, A. Böhmer, L. de’ Medici, M. Capone, G. Giovannetti, R. Eder, L. Wang, M. He, T. Wolf, P. Schweiss *et al.*, *Phys. Rev. B* **94**, 205113 (2016).
- [48] T. Miyake, K. Nakamura, R. Arita, and M. Imada, *J. Phys. Soc. Jpn.* **79**, 044705 (2010).
- [49] N. Lanatà, H. U. R. Strand, G. Giovannetti, B. Hellsing, L. de’ Medici, and M. Capone, *Phys. Rev. B* **87**, 045122 (2013).
- [50] P. Villar Arribi and L. de’ Medici, *Phys. Rev. Lett.* **121**, 197001 (2018).
- [51] A. Liebsch and H. Ishida, *Phys. Rev. B* **82**, 155106 (2010).
- [52] P. Werner, E. Gull, M. Troyer, and A. J. Millis, *Phys. Rev. Lett.* **101**, 166405 (2008).
- [53] L. Fanfarillo and E. Bascones, *Phys. Rev. B* **92**, 075136 (2015).
- [54] S. S. Huh, J. J. Seo, B. S. Kim, S. H. Cho, J. K. Jung, S. Kim, C. I. Kwon, J. S. Kim, Y. Y. Koh, W. S. Kyung *et al.*, *Commun. Phys.* **3**, 52 (2020).
- [55] A. I. Coldea and M. D. Watson, *Annu. Rev. Condens. Matter Phys.* **9**, 125 (2018).
- [56] M. Yi, H. Pfau, Y. Zhang, Y. He, H. Wu, T. Chen, Z. R. Ye, M. Hashimoto, R. Yu, Q. Si, D.-H. Lee, P. Dai, Z.-X. Shen, D. H. Lu, and R. J. Birgeneau, *Phys. Rev. X* **9**, 041049 (2019).
- [57] Y. Suzuki, T. Shimojima, T. Sonobe, A. Nakamura, M. Sakano, H. Tsuji, J. Omachi, K. Yoshioka, M. Kuwata-Gonokami, T. Watashige, R. Kobayashi, S. Kasahara, T. Shibauchi, Y. Matsuda, Y. Yamakawa, H. Kontani, and K. Ishizaka, *Phys. Rev. B* **92**, 205117 (2015).
- [58] K. Nakayama, Y. Miyata, G. N. Phan, T. Sato, Y. Tanabe, T. Urata, K. Tanigaki, and T. Takahashi, *Phys. Rev. Lett.* **113**, 237001 (2014).
- [59] P. Zhang, T. Qian, P. Richard, X. P. Wang, H. Miao, B. Q. Lv, B. B. Fu, T. Wolf, C. Meingast, X. X. Wu, Z. Q. Wang, J. P. Hu, and H. Ding, *Phys. Rev. B* **91**, 214503 (2015).
- [60] S. Bhattacharyya, K. Björnson, K. Zantout, D. Steffensen, L. Fanfarillo, A. Kreisel, R. Valentí, B. M. Andersen, and P. Hirschfeld, *Phys. Rev. B* **102**, 035109 (2020).
- [61] N. Ashcroft and N. Mermin, *Solid State Physics* (Saunders College, Philadelphia, PA, 1976).
- [62] F. Hardy, M. He, L. Wang, T. Wolf, P. Schweiss, M. Merz, M. Barth, P. Adelman, R. Eder, A.-A. Haghighirad *et al.*, *Phys. Rev. B* **99**, 035157 (2019).
- [63] F. Hardy (private communication).
- [64] M. Nakajima, K. Yanase, F. Nabeshima, Y. Imai, A. Maeda, and S. Tajima, *Phys. Rev. B* **95**, 184502 (2017).
- [65] H. Wang, Z. Ye, Y. Zhang, and N. Wang, *Sci. Bull.* **61**, 1126 (2016).
- [66] P. D. Lodhi, N. Kaurav, K. Choudhary, and Y. Kuo, *J. Low Temp. Phys.* **196**, 494 (2019).
- [67] Y. J. Song, J. B. Hong, B. H. Min, Y. S. Kwon, K. J. Lee, M. H. Jung, and J.-S. Rhyee, *J. Korean Phys. Soc.* **59**, 312 (2011).
- [68] T. McQueen, A. Williams, P. Stephens, J. Tao, Y. Zhu, V. Ksenofontov, F. Casper, C. Felser, and R. J. Cava, *Phys. Rev. Lett.* **103**, 057002 (2009).
- [69] J. M. Tomczak and S. Biermann, *Phys. Rev. B* **80**, 085117 (2009).
- [70] B. Valenzuela, M. Calderón, G. León, and E. Bascones, *Phys. Rev. B* **87**, 075136 (2013).
- [71] M. J. Calderón, L. de’ Medici, B. Valenzuela, and E. Bascones, *Phys. Rev. B* **90**, 115128 (2014).
- [72] I. Pallecchi, F. Caglieris, and M. Putti, *Supercond. Sci. Technol.* **29**, 073002 (2016).
- [73] J. Mravlje and A. Georges, *Phys. Rev. Lett.* **117**, 036401 (2016).
- [74] S. Borisenko, D. Evtushinsky, Z.-H. Liu, I. Morozov, R. Kappenberger, S. Wurmehl, B. Büchner, A. Yaresko, T. Kim, M. Hoesch *et al.*, *Nat. Phys.* **12**, 311 (2016).
- [75] Y. Zhang, M. Yi, Z.-K. Liu, W. Li, J. J. Lee, R. G. Moore, M. Hashimoto, M. Nakajima, H. Eisaki, S.-K. Mo, Z. Hussain, T. P. Devereaux, Z.-X. Shen, and D. H. Lu, *Phys. Rev. B* **94**, 115153 (2016).
- [76] M. van Setten, M. Giantomassi, E. Bousquet, M. Verstraete, D. Hamann, X. Gonze, and G.-M. Rignanese, *Comput. Phys. Commun.* **226**, 39 (2018).

- [77] I. Carnimeo, S. Baroni, and P. Giannozzi, *Electron. Struct.* **1**, 015009 (2019).
- [78] L. Lin, *J. Chem. Theory Comput.* **12**, 2242 (2016).
- [79] F. Aryasetiawan and O. Gunnarsson, *Rep. Prog. Phys.* **61**, 237 (1998).
- [80] L. de' Medici and M. Capone, *The Iron Pnictide Superconductors* (Springer, Berlin, 2017), pp. 115–185.
- [81] M. Chatzieftheriou, M. Berović, P. V. Arribi, M. Capone, and L. d' Medici, *Phys. Rev. B* **102**, 205127 (2020).
- [82] M. Hirayama, T. Miyake, M. Imada, and S. Biermann, *Phys. Rev. B* **96**, 075102 (2017).
- [83] P. Reiss, M. Watson, T. Kim, A. Haghighirad, D. Woodruff, M. Bruma, S. Clarke, and A. Coldea, *Phys. Rev. B* **96**, 121103 (2017).
- [84] T. Shimojima, Y. Suzuki, T. Sonobe, A. Nakamura, M. Sakano, J. Omachi, K. Yoshioka, M. Kuwata-Gonokami, K. Ono, H. Kumigashira, A. E. Böhmer, F. Hardy, T. Wolf, C. Meingast, H. v. Löhneysen, H. Ikeda, and K. Ishizaka, *Phys. Rev. B* **90**, 121111 (2014).